Electronic Supplementary Material (ESI) for Journal of Materials Chemistry C.

Modulating crystal packing to achieve efficient ultralong organic phosphorescence by simple methylation engineering

Huiting Mao,[a,b] Jing Gao,[c] Yun Geng,[c] Guo-Gang Shan,*[c] Kuizhan Shao,[c] Ruinian Hua*[a] and Zhongmin Su*[b]

[a]College of Life Science, Dalian Minzu University, Dalian, 116600, China, E-mail: rnhua@dlnu.edu.cn

[b]State Key Laboratory of Supramolecular Structure and Materials, Institute of Theoretical Chemistry, College of Chemistry, Jilin University, Changchun, Jilin, 130012, China, E-mail: zmsu@nenu.edu.cn

[c]National & Local United Engineering Laboratory for Power Batteries, Department of Chemistry, Northeast Normal University, Changchun, Jilin, 130024, China,
E-mail: shangg187@nenu.edu.cn(G. S.)

I. Experimental section

Reagents and materials

Unless otherwise noted, all reagents used in the experiments were purchased from commercial sources without further purification. For column chromatography, silica gel with 300~400 mesh was used. These compounds were synthesized according to the similar experimental procedures reported previously.

Measurements

Nuclear magnetic resonance (^{1}H and ^{13}C NMR) spectra were obtained on a Bruker Avance 500 MHz spectrometer. High-resolution mass spectra (HRMS) were tested on Bruck microtof or Hybrid Quadrupole-Orbitrap GC-MS/MS system (Q Exactive GC). X-ray crystallography was measured by a Bruker Apex CCD II area-detector diffractometer. Ultraviolet absorption spectra were obtained by Cary 500 UV-Vis-NIR spectrophotometer. Steady-state photoluminescence (PL) and phosphorescence spectra were measured using FL-4600 FL spectrophotometer. The lifetime and time-resolved emission spectra were obtained on FLSP920 Edinburgh Fluorescence Spectrometer equipped with a xenon arc lamp (Xe900), a nanosecond hydrogen flash-lamp (nF920), and a microsecond flash-lamp (μF900), respectively. **Computational details**

All studied geometrical, electronic structures and relevant photophysical properties were explored in the Gaussian 16[1] and ADF 2016[2] program packages. We used 6-31G** basis set for all the atoms and B3LYP functional to optimize the structures of the monomers and dimers selected from the experimental crystals. Considering the intermolecular interaction effects, the quantum mechanics/molecular mechanics (QM/MM) method using the ONIOM model with electronic embedding were employed to optimize geometrical structures.[3] The chosen monomers and dimers are treated calculated at the QM level while the surrounding molecules are calculated at the MM level. We select the density functional theory (DFT) and time-dependent density functional theory (TDDFT) for central molecules at the ground state and excited state, respectively.[4] The surrounding molecules are calculated by the

universal force field (UFF).[5] The ADF 2016 program package was employed to calculate the spin-orbital coupling (SOC) matrix element values of the monomers and dimers with the B3LYP functional and the ZORA/DZP basis set.[6]

The preparation of anti-counterfeiting and 3D patterns

Firstly, the ink based on material *m*-DMOPP was prepared with aloe vera gel. The ink was then printed onto a piece of black paper with screen printing technique. After heat treatment for 30 minutes, a "Fu" pattern with UOP feature was obtained. A bright blue pattern of "Fu" was clearly visualized under 365 nm UV-lamp irradiation. "Fu" with green emission can be observed by the naked-eye after removing the excitation light source. ***m*-DMOPP** microcrystals (10 mg) was doped into PDMS (10 mL) to afford RTP gel for 3D patterns.

II. Synthesis and characterization of these compounds

Synthesis of **10-phenyl-10*H*-phenothiazine 5,5-dioxide (OPP)**. Phenothiazine (2.00 g, 10 mmol), iodobenzene (2.26 g, 12 mol), potassium tert-butoxide (1.69 g, 15 mmol), palladium acetate (0.11 g, 0.5 mmol), and tri-tert-butylphosphine (0.5 mL, 0.25 mmol) were dissolved in toluene (100 mL) in a round-bottom flask. Then the mixture was stirred at 110 ^{o}C under argon. After 12 hours, the reaction mixture was extracted with CH_2Cl_2 three times. Then the organic layer was collected and dried with Na_2SO_4. The solvent was removed by rotary evaporation, and the residue was purified by column chromatography. Then the collected product was added to CH_2Cl_2 (90 mL), acetic acid (45 mL), and H_2O_2 (2 mL). After stirring for 24 hours at 60 ^{o}C, the mixture was extracted with CH_2Cl_2 and further purified by column chromatography, affording a white solid with a yield of 82%. ^{1}H NMR (600 MHz, $CDCl_3$, δ [ppm]): 8.17 (dd, J = 7.8, 1.2 Hz, 2H), 7.69-7.71 (m, 2H), 7.62-7.64 (m, 1H), 7.37-7.39 (m, 4H), 7.23-7.26 (m, 2H), 6.62 (d, J = 8.4 Hz, 2H). ^{13}C NMR (150 MHz, $CDCl_3$, δ [ppm]): 140.78, 138.92, 132.76, 131.36, 130.48, 129.76, 123.41, 122.61, 122.04, 117.23. MS [m/z]: Calcd for $C_{18}H_{13}NO_2S$: 307.0667, Found 330.0550 [M + Na]$^{+}$.

Synthesis of **10-(o-tolyl)-10*H*-phenothiazine 5,5-dioxide (*o*-MOPP)**. White solid

(yield: 80%). ^{1}H NMR (600 MHz, $CDCl_3$, δ [ppm]): 8.19 (d, J = 8.4 Hz, 2H), 7.48-7.53 (m, 3H), 7.39-7.41 (m, 2H), 7.30 (d, J = 7.8 Hz, 1H), 7.24-7.26 (m, 2H), 6.55 (d, J = 9.0 Hz, 2H), 2.01 (s, 3H). ^{13}C NMR (150 MHz, $CDCl_3$, δ [ppm]): 139.75, 138.15, 137.21, 133.05, 132.72, 130.51, 130.01, 128.68, 123.55, 122.63, 122.08, 116.57, 17.04. MS [m/z]: Calcd for $C_{19}H_{15}NO_2S$: 321.0823, Found 344.0707 $[M + Na]^+$.

Synthesis of **10-(m-tolyl)-10*H*-phenothiazine 5,5-dioxide (*m*-MOPP)**. White solid (yield: 82%). ^{1}H NMR (600 MHz, $CDCl_3$, δ [ppm]): 8.15-8.17 (m, 2H), 7.55-7.58 (m, 1H), 7.42 (d, J = 7.8 Hz, 1H), 7.37-7.39 (m, 2H), 7.23 (t, J = 7.2 Hz, 2H), 7.18 (s, 2H), 6.65 (d, J = 9.0 Hz, 2H), 2.46 (s, 3H). ^{13}C NMR (150 MHz, $CDCl_3$, δ [ppm]): 141.78, 140.78, 138.80, 132.71, 130.96, 130.77, 130.45, 127.31, 123.35, 122.54, 121.95, 117.33, 21.39. MS [m/z]: Calcd for $C_{19}H_{15}NO_2S$: 321.0823, Found 344.0707 $[M + Na]^+$.

Synthesis of **10-(2,6-dimethylphenyl)-10*H*-phenothiazine 5,5-dioxide (*o*-DMOPP)**. White solid (yield: 60%). ^{1}H NMR (500 MHz, $CDCl_3$, δ [ppm]): 8.21 (dd, J = 8.0, 1.5 Hz, 2H), 7.40-7.43 (m, 3H), 7.33 (d, J = 7.5 Hz, 2H), 7.24-7.27 (m, 2H), 6.51 (d, J = 8.5 Hz, 2H), 1.99 (s, 6H). ^{13}C NMR (125 MHz, $CDCl_3$, δ [ppm]): 138.56, 137.92, 135.77, 133.32, 129.86, 129.70, 123.64, 122.61, 122.09, 115.71, 17.44. MS [m/z]: Calcd for $C_{20}H_{17}NO_2S$: 335.0980, Found 358.0866 $[M + Na]^+$.

Synthesis of **10-(3,5-dimethylphenyl)-10*H*-phenothiazine 5,5-dioxide (*m*-DMOPP)**. White solid (yield: 78%). ^{1}H NMR (500 MHz, $CDCl_3$, δ [ppm]): 8.21 (dd, J = 7.0, 1.5 Hz, 2H), 7.37-7.40 (m, 2H), 7.21-7.24 (m, 3H), 6.98 (s, 2H), 6.68 (d, J = 7.0 Hz, 2H), 2.42 (s, 6H). ^{13}C NMR (150 MHz, $CDCl_3$, δ [ppm]): 141.31, 140.76, 138.68, 132.67, 131.25, 127.67, 123.29, 122.45, 121.85, 117.42, 21.32. MS [m/z]: Calcd for $C_{20}H_{17}NO_2S$: 335.0980, Found 358.0864 $[M + Na]^+$.

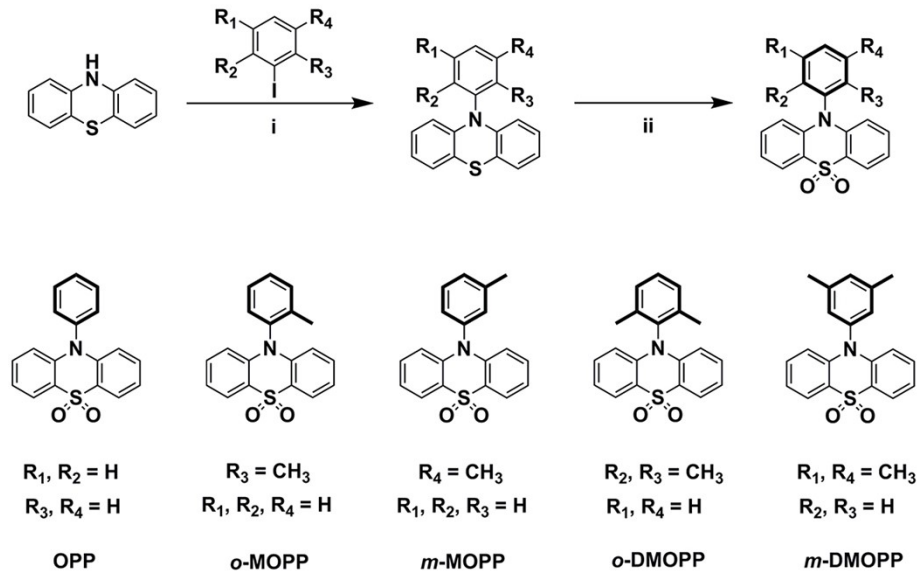

Scheme S1. Synthetic routes and chemical structures of **OPP**, ***o*-MOPP**, ***m*-MOPP**, ***o*-DMOPP**, and ***m*-DMOPP**. i) *t*-BuOK, $Pd(OAc)_2$, P(*t*-Bu)$_3$, Toluene, 110 °C. ii) H_2O_2, CH_2Cl_2/CH_3COOH, 60 °C.

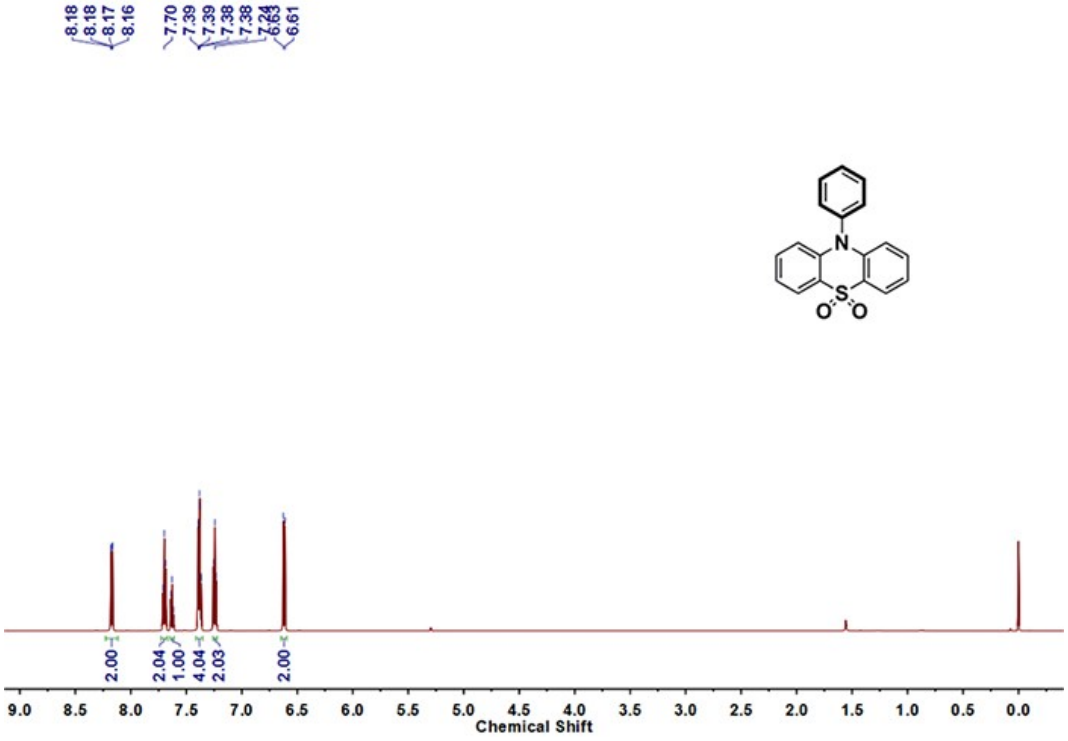

Figure S1. ^{1}H NMR spectrum of **OPP** in $CDCl_3$.

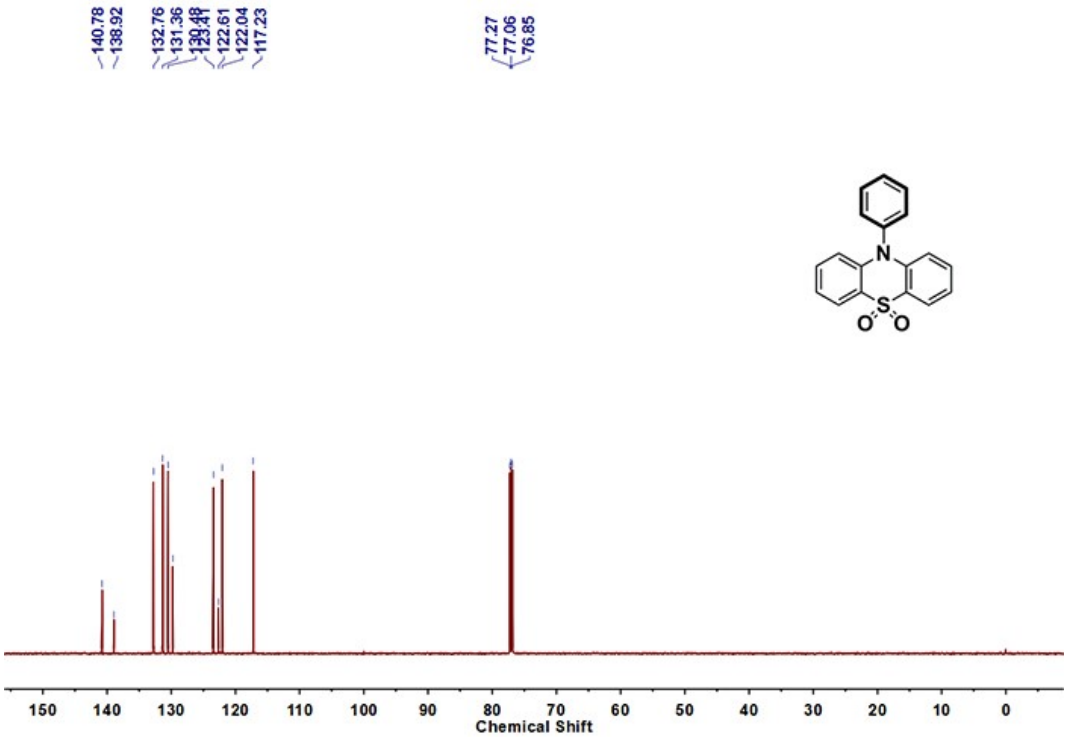

Figure S2. ^{13}C NMR spectrum of **OPP** in $CDCl_3$.

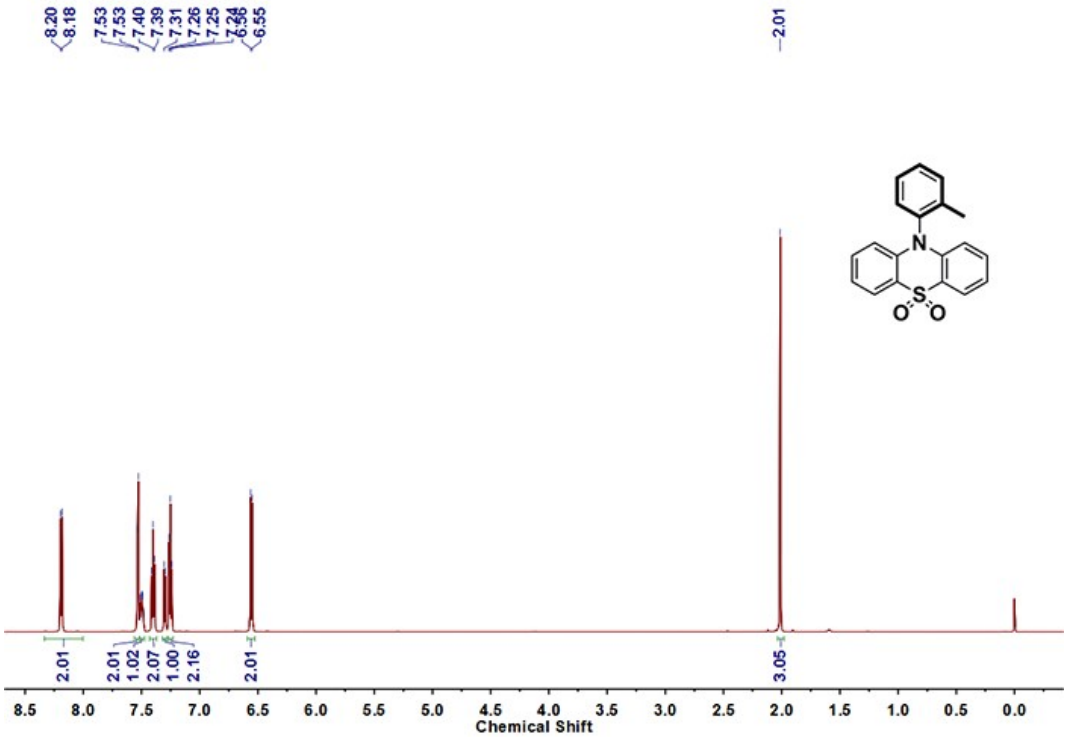

Figure S3. ^{1}H NMR spectrum of ***o*-MOPP** in $CDCl_3$.

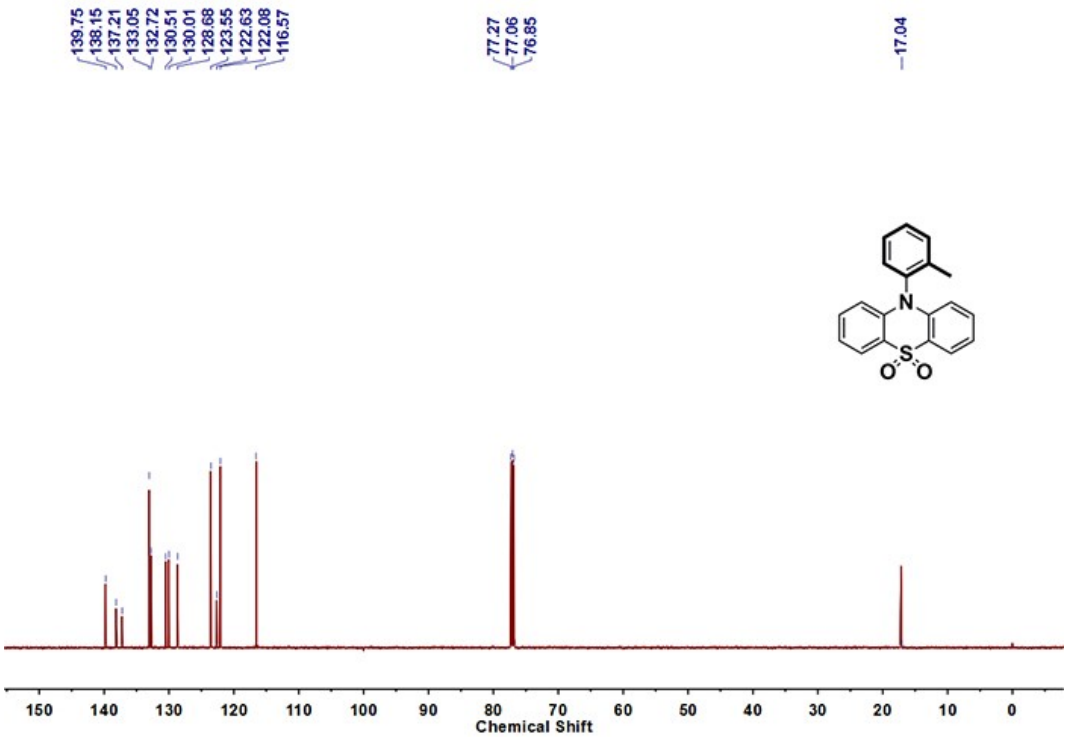

Figure S4. ^{13}C NMR spectrum of ***o*-MOPP** in $CDCl_3$.

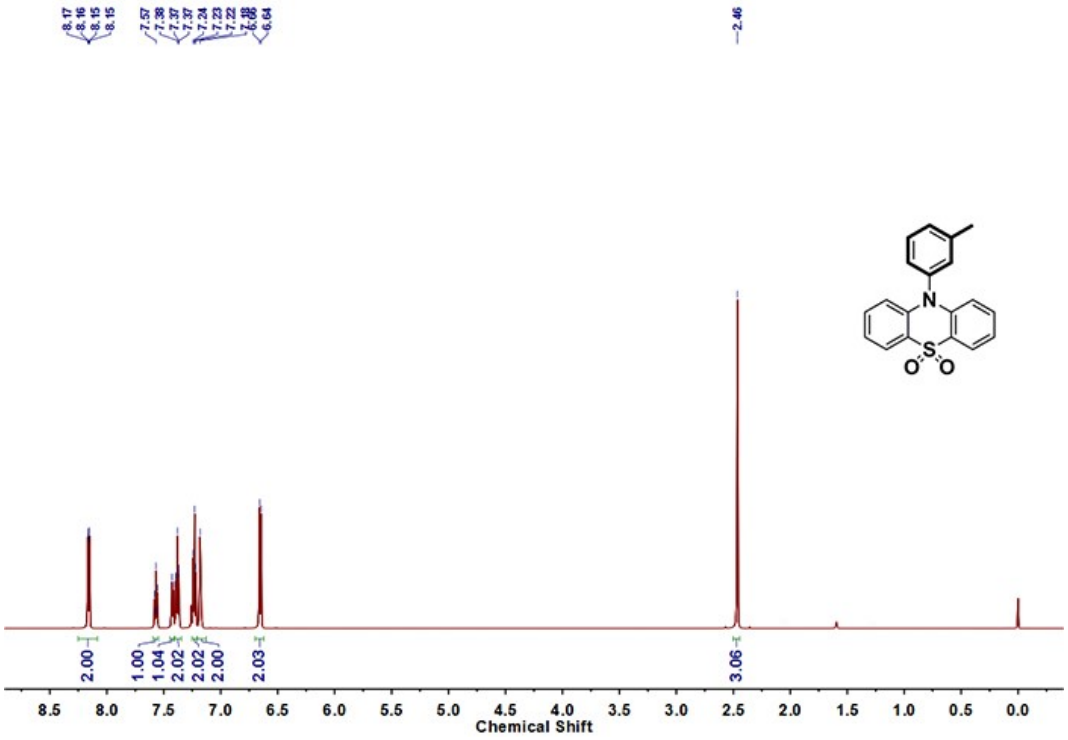

Figure S5. ^{1}H NMR spectrum of ***m*-MOPP** in $CDCl_3$.

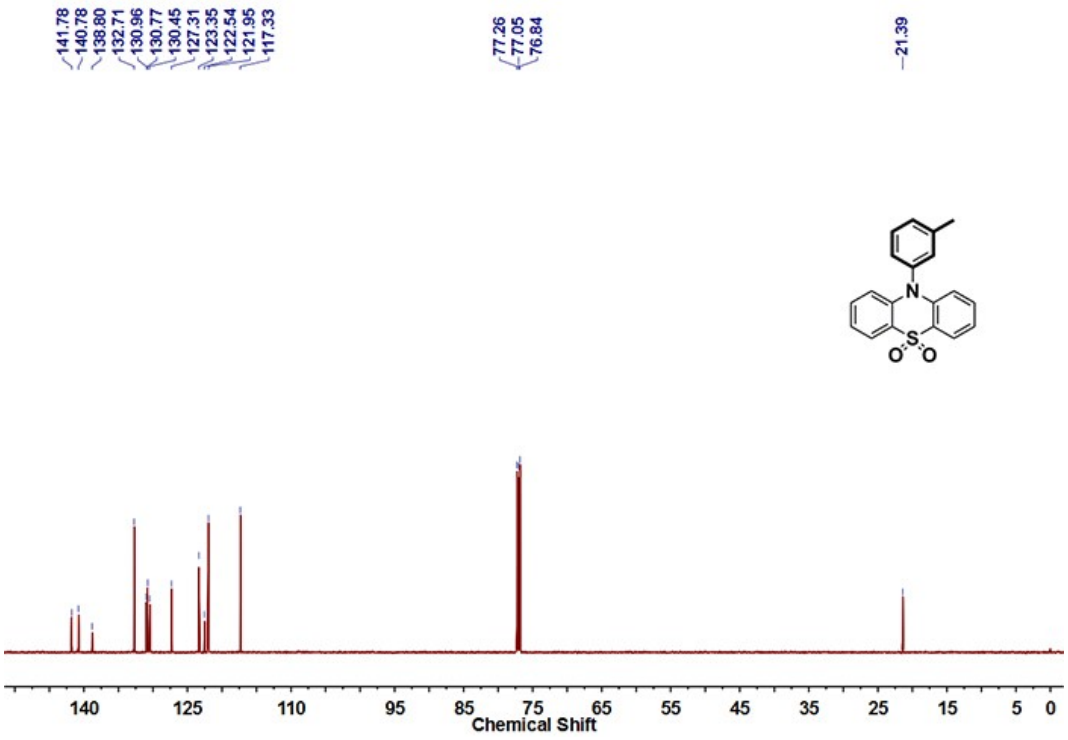

Figure S6. ^{13}C NMR spectrum of ***m*-MOPP** in $CDCl_3$.

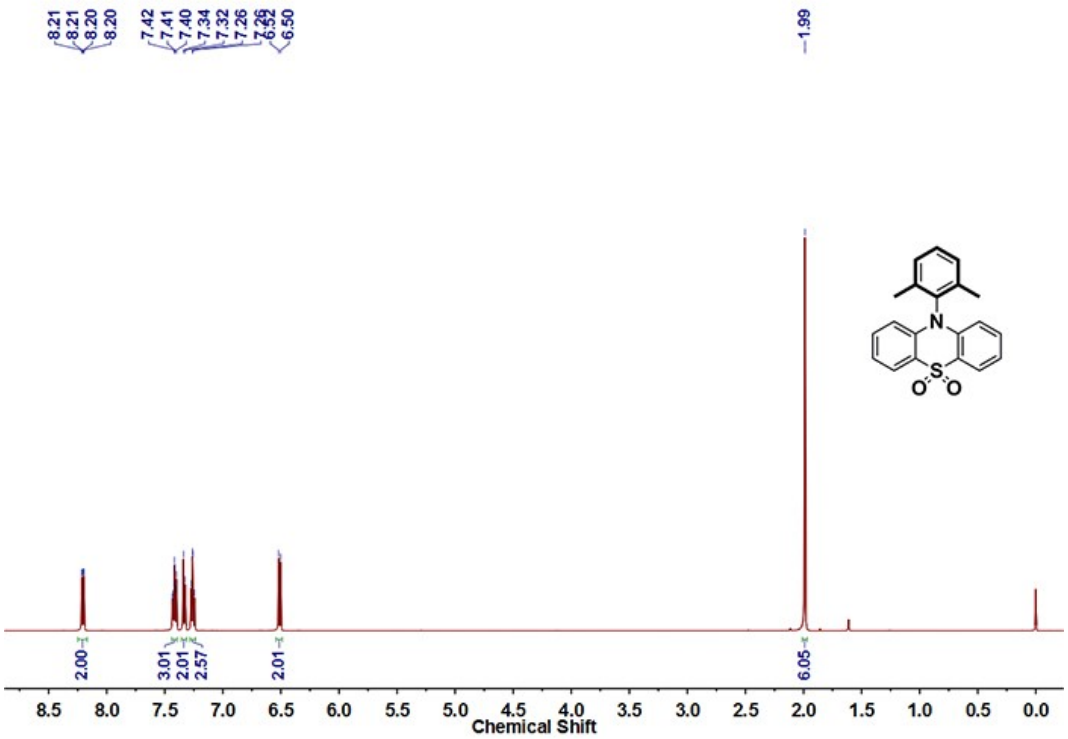

Figure S7. ^{1}H NMR spectrum of ***o*-DMOPP** in $CDCl_3$.

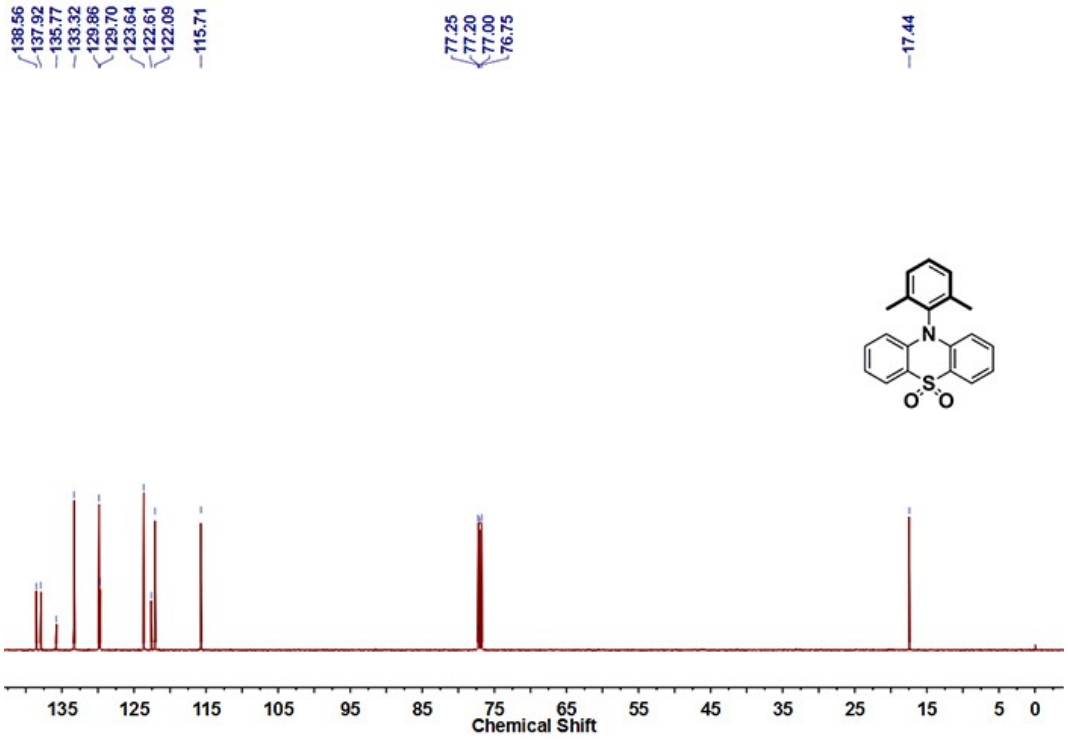

Figure S8. ^{13}C NMR spectrum of ***o*-DMOPP** in $CDCl_3$.

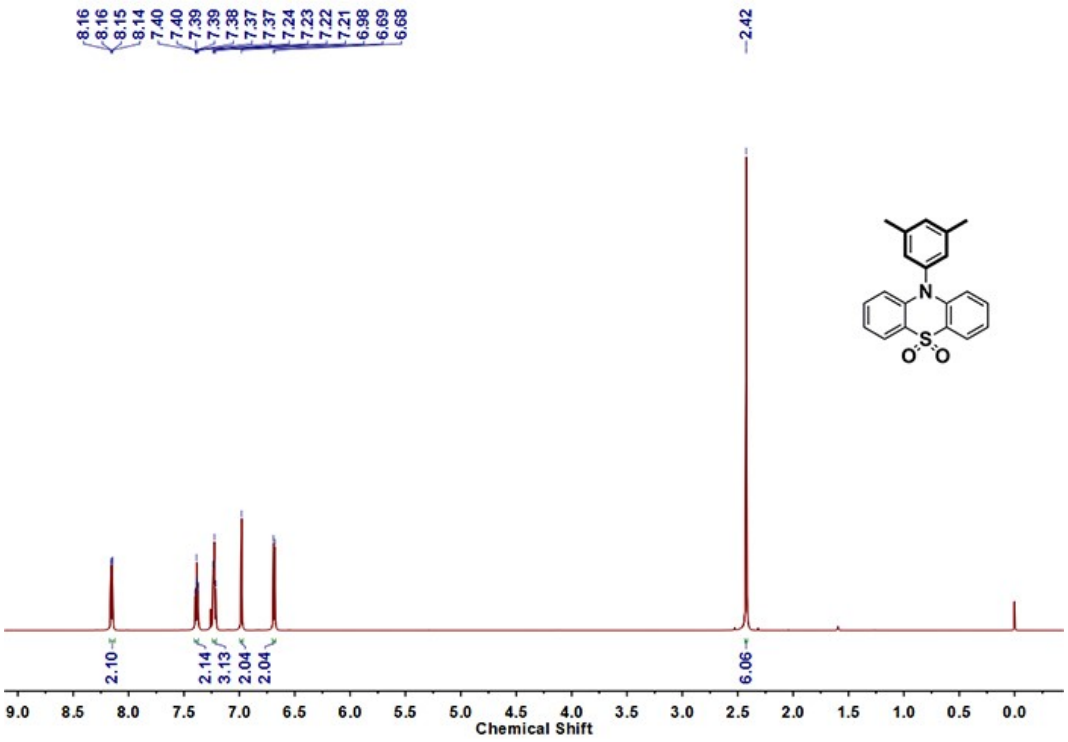

Figure S9. ^{1}H NMR spectrum of ***m*-DMOPP** in $CDCl_3$.

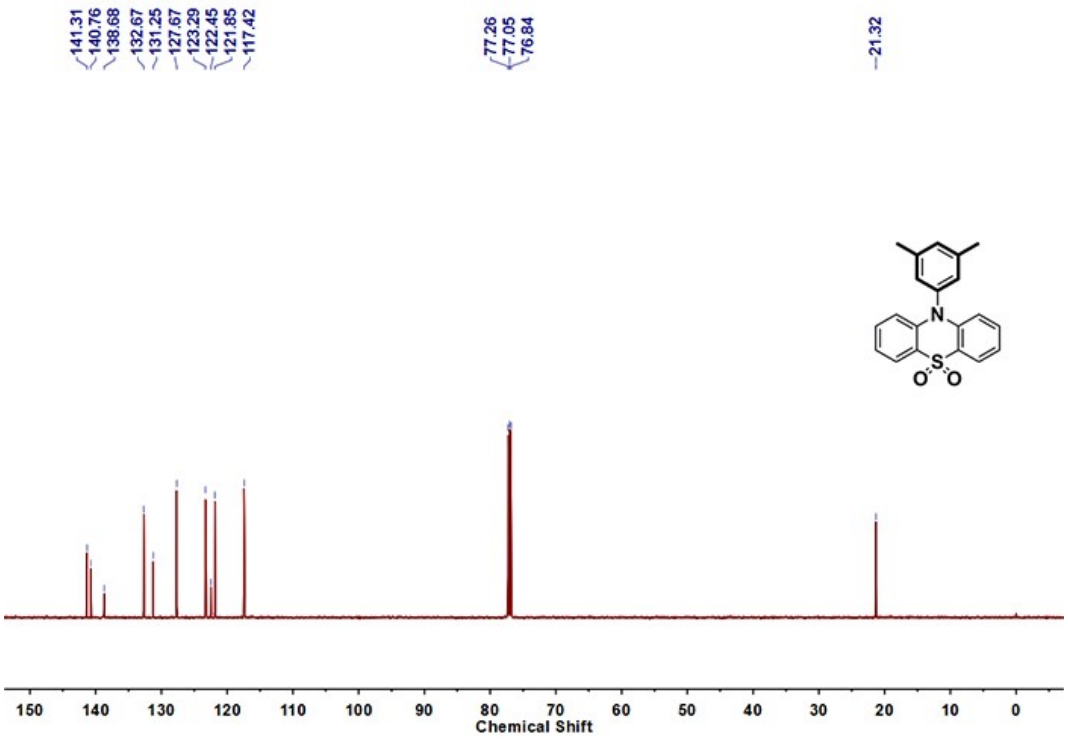

Figure S10. ^{13}C NMR spectrum of ***m*-DMOPP** in $CDCl_3$.

III. Supplementary photophysical properties of the compounds in solution and crystal states

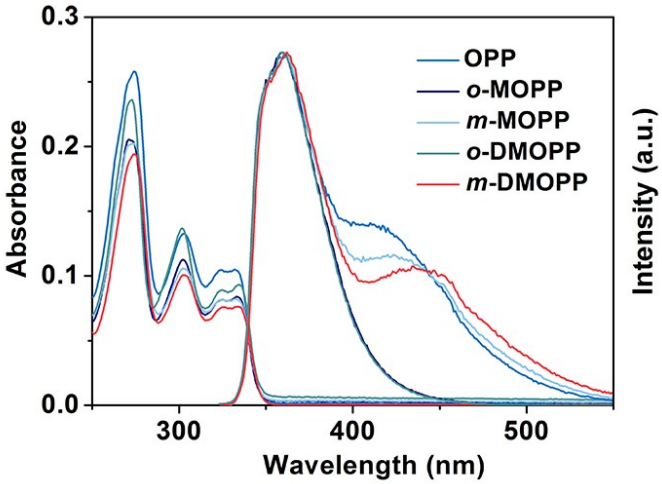

Figure S11. The UV-visible and steady-state PL spectra of **OPP**, ***o*-MOPP**, ***m*-MOPP**, ***o*-DMOPP**, and ***m*-DMOPP** in dilute dichloromethane solutions (10^{-5} M) under ambient conditions.

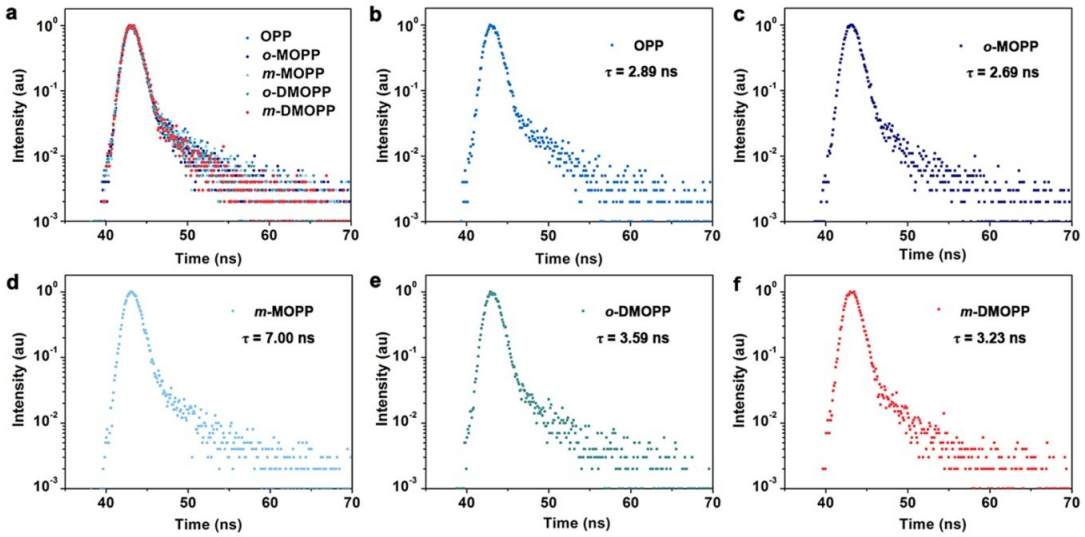

Figure S12. Fluorescence lifetime decay profiles of a) all compounds, b) **OPP** (362 nm), c) ***o*-MOPP** (359 nm), d) ***m*-MOPP** (362 nm), e) ***o*-DMOPP** (359 nm), and f) ***m*-DMOPP** (362 nm) in dilute dichloromethane solutions under ambient conditions.

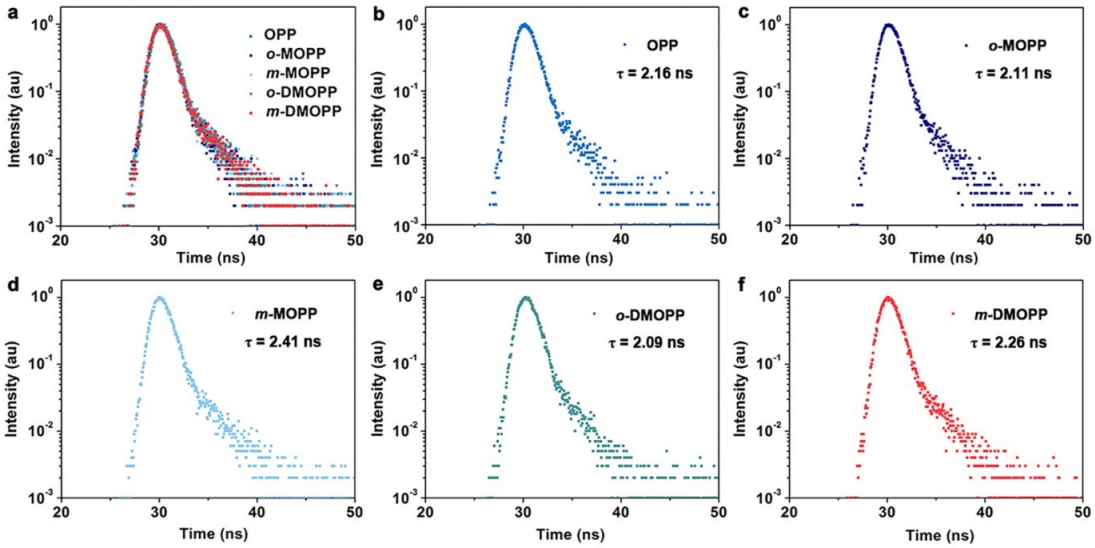

Figure S13. Fluorescence lifetime decay profiles of a) all compounds, b) **OPP** (386 nm), c) ***o*-MOPP** (383 nm), d) ***m*-MOPP** (375 nm), e) ***o*-DMOPP** (370 nm), and f) ***m*-DMOPP** (372 nm) in crystal state.

Table S1. Summarized photophysical data of **OPP**, ***o*-MOPP**, ***m*-MOPP**, ***o*-DMOPP**, and ***m*-DMOPP** in crystal state at 298 K.

Compound	λ_F (nm)	τ_F (ns)	λ_P (nm)	τ_P (ms)	Φ_P (%)	k_{isc} (s^{-1})	k_r (s^{-1})	k_{nr} (s^{-1})
OPP	386	2.16	517	185	0.5	2.3×10^6	2.7×10^{-2}	5.38
***o*-MOPP**	383	2.11	508	245	0.3	1.4×10^6	1.2×10^{-2}	4.07
***m*-MOPP**	375	2.41	525	335	0.8	3.3×10^6	2.4×10^{-2}	2.96
***o*-DMOPP**	370	2.09	518	357	1.4	6.7×10^6	3.9×10^{-2}	2.76
***m*-DMOPP**	372	2.26	512	375	1.9	8.4×10^6	5.0×10^{-2}	2.62

λ_F: fluorescent emission peak; τ_F: fluorescent lifetime; λ_P: phosphorescent emission peak; τ_F: phosphorescent lifetime; Φ_P: quantum yield.

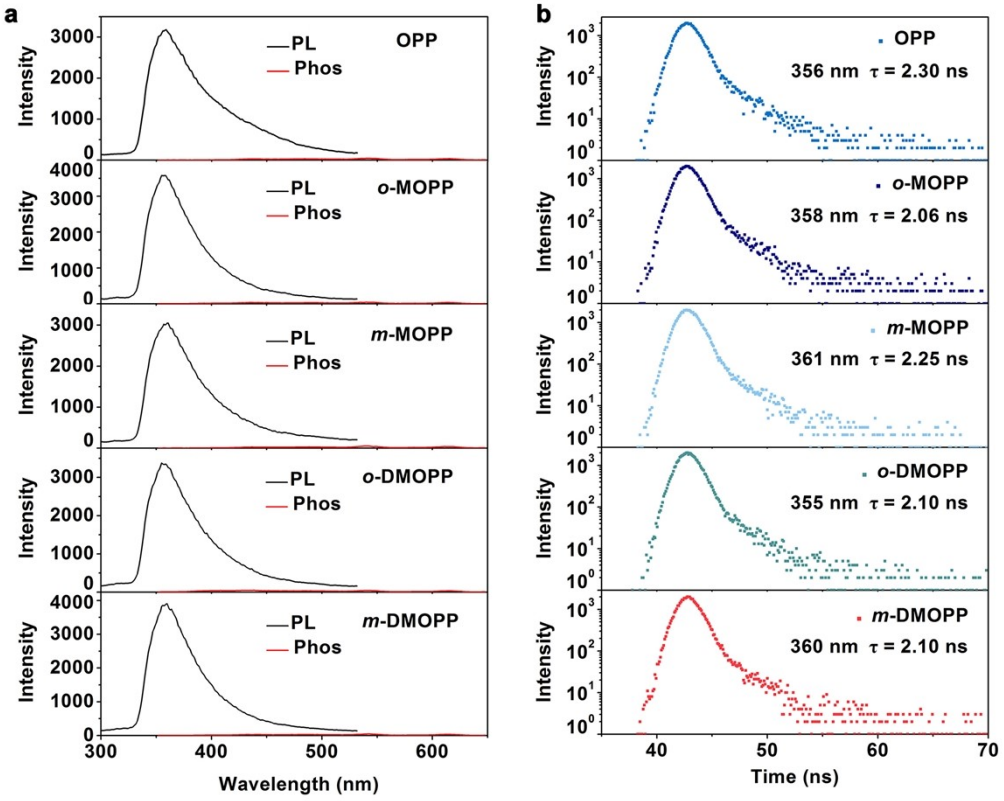

Figure S14. a) Steady-state photoluminescence (PL) (black line) and phosphorescence (Phos) spectra (red line) and b) the time-resolved fluorescence decay curves of **OPP**, ***o*-MOPP**, ***m*-MOPP**, ***o*-DMOPP**, and ***m*-DMOPP** doped in PMMA films (5 wt%) under ambient conditions with an excitation wavelength of 330 nm.

IV. Single crystal data

Table S2. Crystal data and structure refinement of all compounds.

Name	**OPP**	***o*-MOPP**	***m*-MOPP**	***o*-DMOPP**	***m*-DMOPP**
CCDC	2041000	2041001	2041002	2041003	2041004
Formula	$C_{18}H_{13}NO_2S$	$C_{19}H_{15}NO_2S$	$C_{19}H_{15}NO_2S$	$C_{20}H_{17}NO_2S$	$C_{20}H_{17}NO_2S$
Formula weight	307.35	321.38	321.38	335.42	335.40
Crystal system	Monoclinic	Monoclinic	Monoclinic	Monoclinic	Monoclinic
Space group	$P2_1/n$	$P2_1/c$	$P2_1/n$	$P2_1/n$	C2/c
Cell Lengths (Å)	a 9.0074(16) b 13.082(2) c 12.862(2)	a 9.4141(12) b 19.321(3) c 8.6620(11)	a 8.9570(12) b 14.1439(17) c 12.4792(15)	a 7.2656(5) b 18.9739(11) c 12.0131(9)	a 16.1938(10) b 8.0950(5) c 25.4630(16)
Cell Angles (°)	α 90 β 104.033(6) γ 90	α 90 β 105.449(5) γ 90	α 90 β 103.209(4) γ 90	α 90 β 93.825(4) γ 90	α 90 β 98.695(3) γ 90
Cell Volume (Å^3)	1470.4(4)	1518.6(3)	1539.1(3)	1652.40(19)	3299.6(4)
Z	4	4	4	4	8
$D_{calcd.}$(g m^{-3})	1.388	1.406	1.387	1.348	1.350
F(000)	640.0	672.0	672.0	704.4	1408.0
R_{int}	0.0543	0.0336	0.0461	0.0479	0.0413
F^2	1.170	1.077	1.142	1.083	1.212
R_1[a], wR_2[b]	0.0497,0.1278	0.0404,0.0974	0.0605,0.1312	0.0486,0.1133	0.0663,0.1662

R_1, wR_2	0.0801,0.1542	0.0449,0.1002	0.0815,0.1465	0.0704,0.1275	0.0697,0.1704

[a] $R_1 = \Sigma||F_o|-|F_c||/\Sigma|F_o|$. [b] $wR_2 = |\Sigma w(|F_o|^2-|F_c|^2)|/\Sigma|w(F_o^2)^2|^{1/2}$.

Table S3. The types and distance of intermolecular interactions for **OPP**, ***o*-MOPP**, ***m*-MOPP**, ***o*-DMOPP**, and ***m*-DMOPP** crystals.

OPP		***o*-MOPP**		***m*-MOPP**		***o*-DMOPP**		***m*-DMOPP**	
Types of bond	distance (Å)	Types of bond	distance (Å)	Types of bond	distance (Å)	Types of bond	distance (Å)	Types of bond	distance (Å)
C-H...O	2.408	C-H...O	2.474	C-H...O	2.589	C-H...O	2.713	C-H...O	2.529
C-H...O	2.537	C-H...O	2.574	C-H...O	2.595	C-H...π	2.814	C-H...O	2.591
C-H...π	2.832	C-H...O	2.650	C-H...O	2.612	S=O...C	3.210	C-H...O	2.644
C-H...π	2.860	C-H...π	2.869	C-H...π	2.804			S=O...C	3.140
C-H...π	2.870	C-H...H-C	2.359	C-H...π	2.836				
S=O...C	3.171	C-H...C	2.871	C-H...π	2.888				

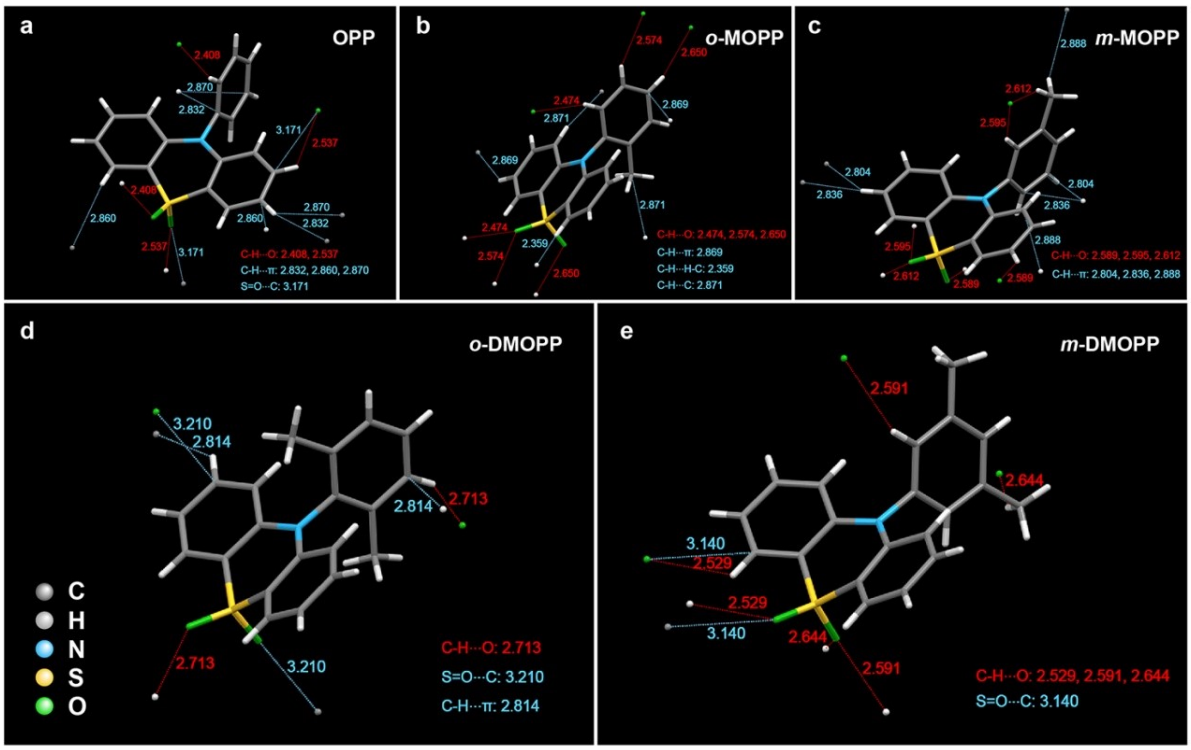

Figure S15. a) The intermolecular interactions of a) **OPP**, b) ***o*-MOPP**, c) ***m*-MOPP**, d) ***o*-DMOPP**, and e) ***m*-DMOPP** in crystal states.

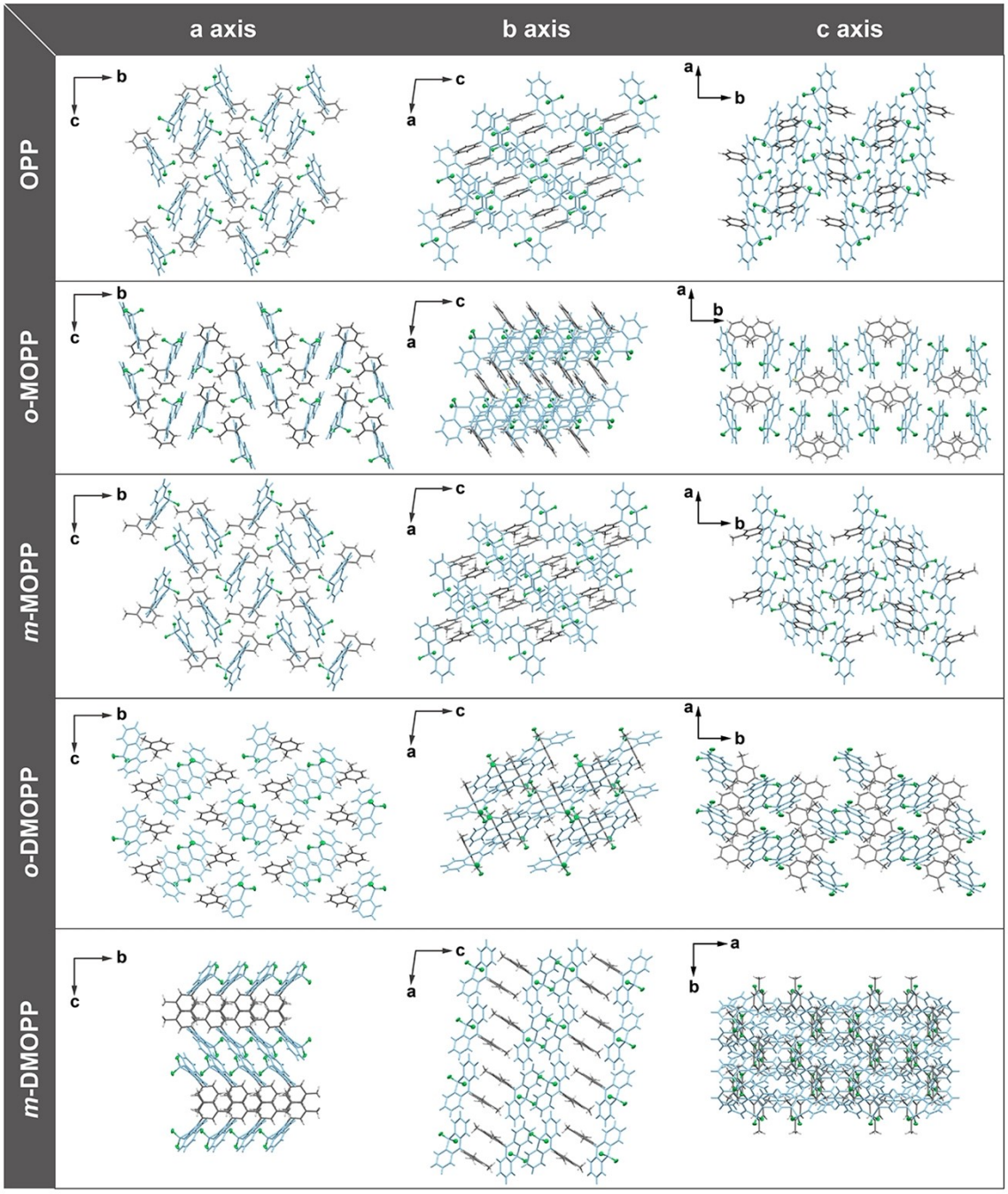

Figure S16. a) Packing diagrams along a, b, and c axis for **OPP**, ***o*-MOPP**, ***m*-MOPP**, ***o*-DMOPP**, and ***m*-DMOPP** crystals.

V. Theoretical calculations

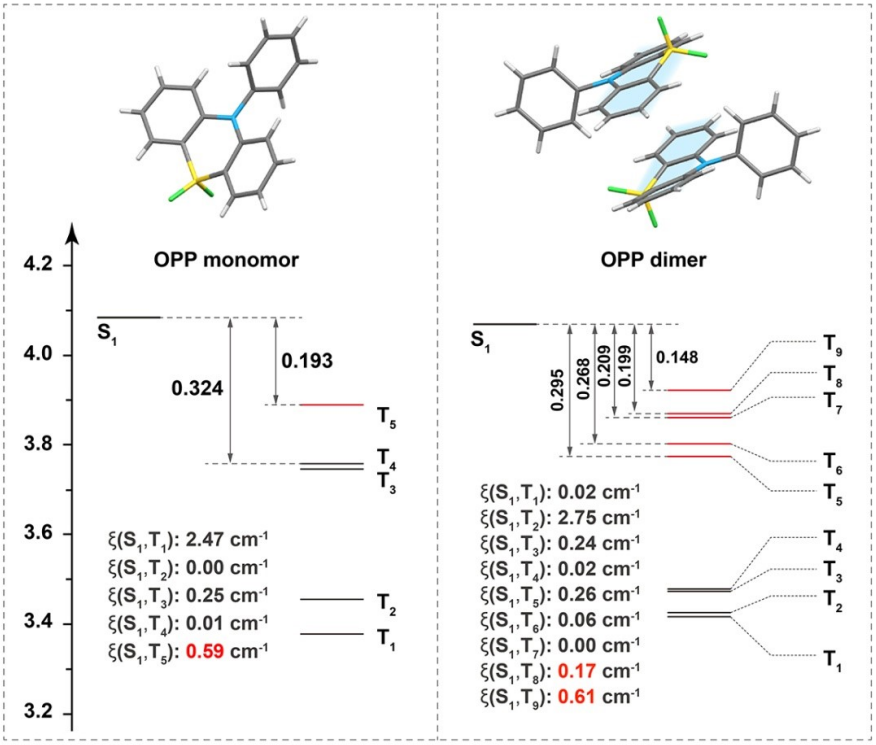

Figure S17. Calculated energy gaps and spin-orbit coupling constant (ξ) between S_1 and T_n for **OPP** monomer and dimer.

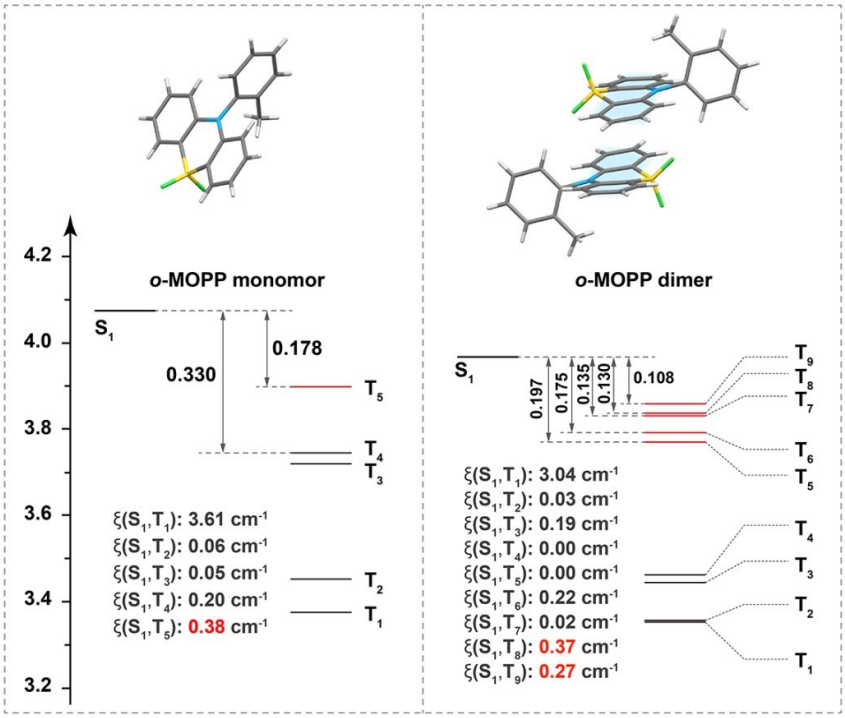

Figure S18. Calculated energy gaps and spin-orbit coupling constant (ξ) between S_1 and T_n for ***o*-MOPP** monomer and dimer.

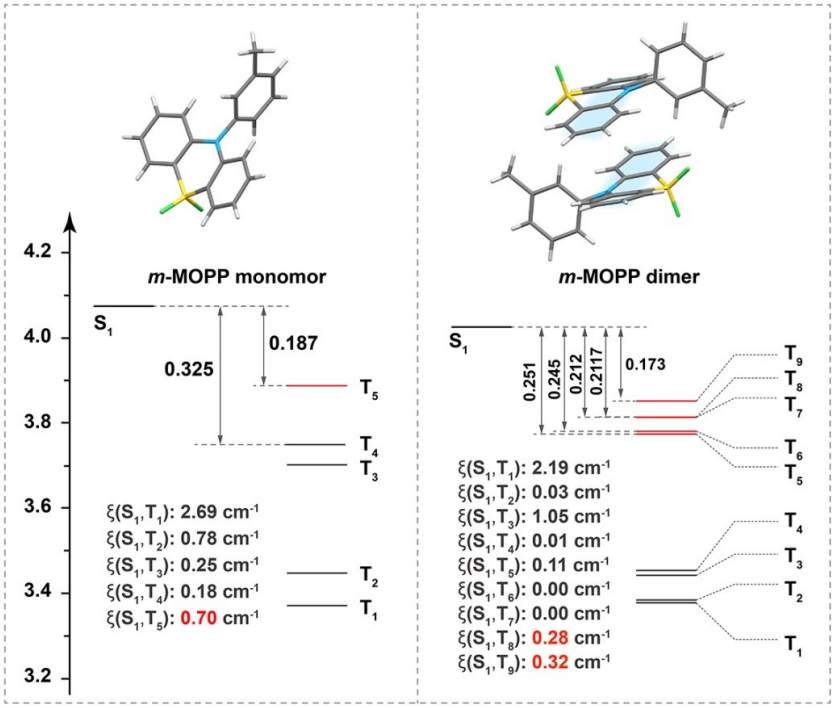

Figure S19. Calculated energy gaps and spin-orbit coupling constant (ξ) between S_1 and T_n for ***m*-MOPP** monomer and dimer.

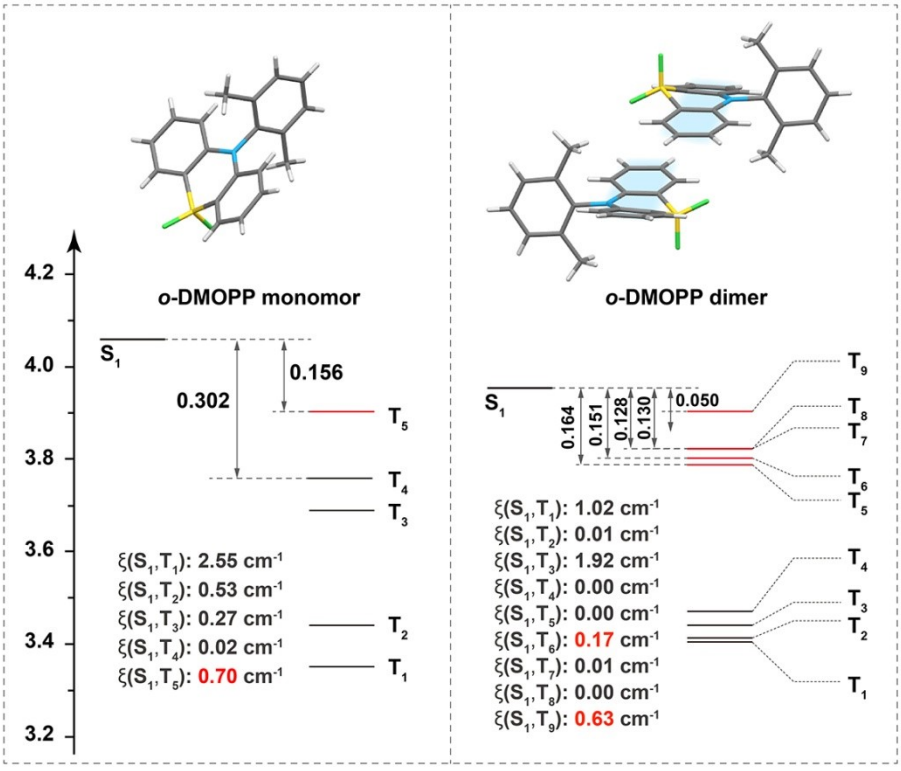

Figure S20. Calculated energy gaps and spin-orbit coupling constant (ξ) between S_1 and T_n for ***o*-DMOPP** monomer and dimer.

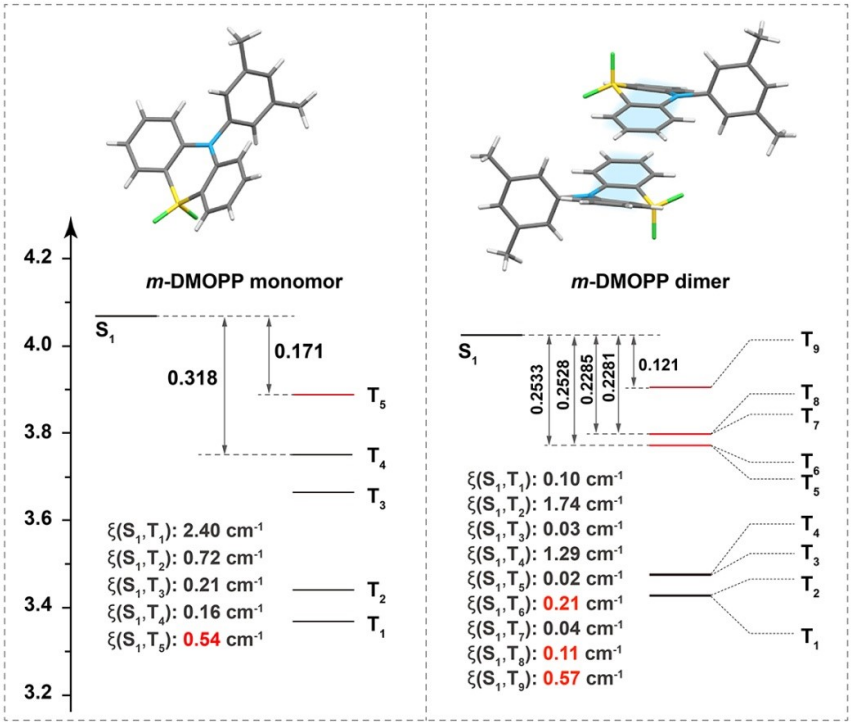

Figure S21. Calculated energy gaps and spin-orbit coupling constant (ξ) between S_1 and T_n for ***m*-DMOPP** monomer and dimer.

Table S4. Calculated spin-orbit coupling constant (ξ) (cm^{-1}) of these compounds in the single molecules and dimers.

		OPP	***o*-MOPP**	***m*-MOPP**	***o*-DMOPP**	***m*-DMOPP**
Monomer	S_1-T_1	2.47	3.61	2.69	2.55	2.4
	S_1-T_2	0.004	0.06	0.78	0.53	0.72
	S_1-T_3	0.25	0.05	0.25	0.27	0.21
	S_1-T_4	0.01	0.20	0.18	0.02	0.16
	S_1-T_5	0.59	0.38	0.70	0.70	0.54
Dimer	S_1-T_1	0.016	3.04	2.19	1.02	0.10
	S_1-T_2	2.75	0.03	0.03	0.01	1.74
	S_1-T_3	0.239	0.19	1.05	1.92	0.03
	S_1-T_4	0.019	0.00	0.01	0.00	1.29
	S_1-T_5	0.258	0.00	0.11	0.00	0.02
	S_1-T_6	0.06	0.22	0.00	0.17	0.21
	S_1-T_7	0.003	0.02	0.00	0.01	0.04

	S_1-T_8	0.167	0.37	0.28	0.00	0.11
	S_1-T_9	0.609	0.27	0.32	0.63	0.57

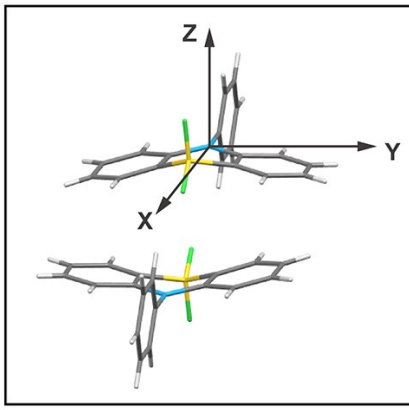

Compound	S_X (Å)	S_Y (Å)	S_Z (Å)
OPP	2.977	1.203	4.156
***o*-MOPP**	4.531	0.166	3.467
***m*-MOPP**	2.897	1.304	3.943
***o*-DMOPP**	5.549	2.556	3.368
***m*-DMOPP**	4.442	2.646	3.440

Figure S22. The Cartesian coordinates in the simulated dimer for ***o*-MOPP** and the shift along X, Y, and Z axis of one molecule relative to another molecule in the selected dimers from different crystals. The N atom is set as the coordinate origin, and N-C bond connected to phenyl is in the x axis.

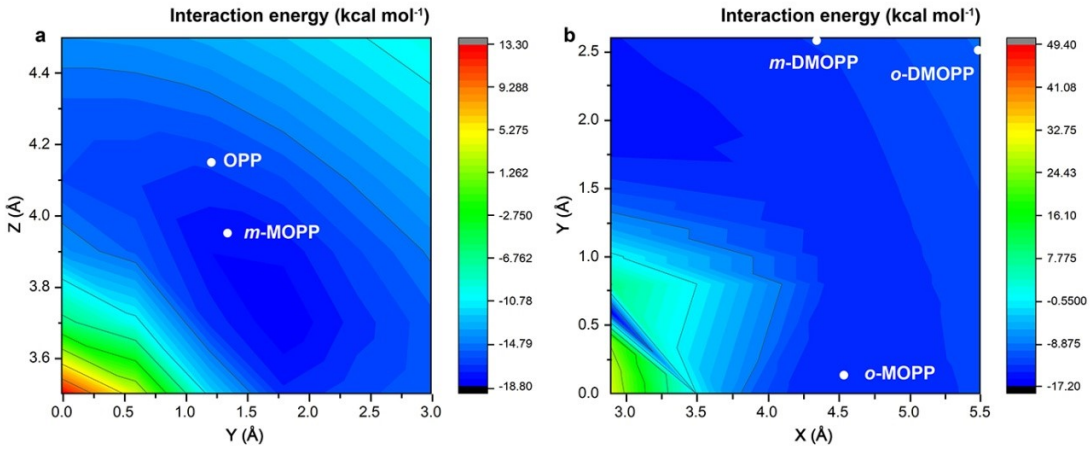

Figure S23. The change of intermolecular interaction energy (kcal mol^{-1}) with the shift of relative position in the simulated dimer. The shift along the X-axis is set as 2.9 Å a) and the shift along the Z-axis is set as 3.4 Å b).

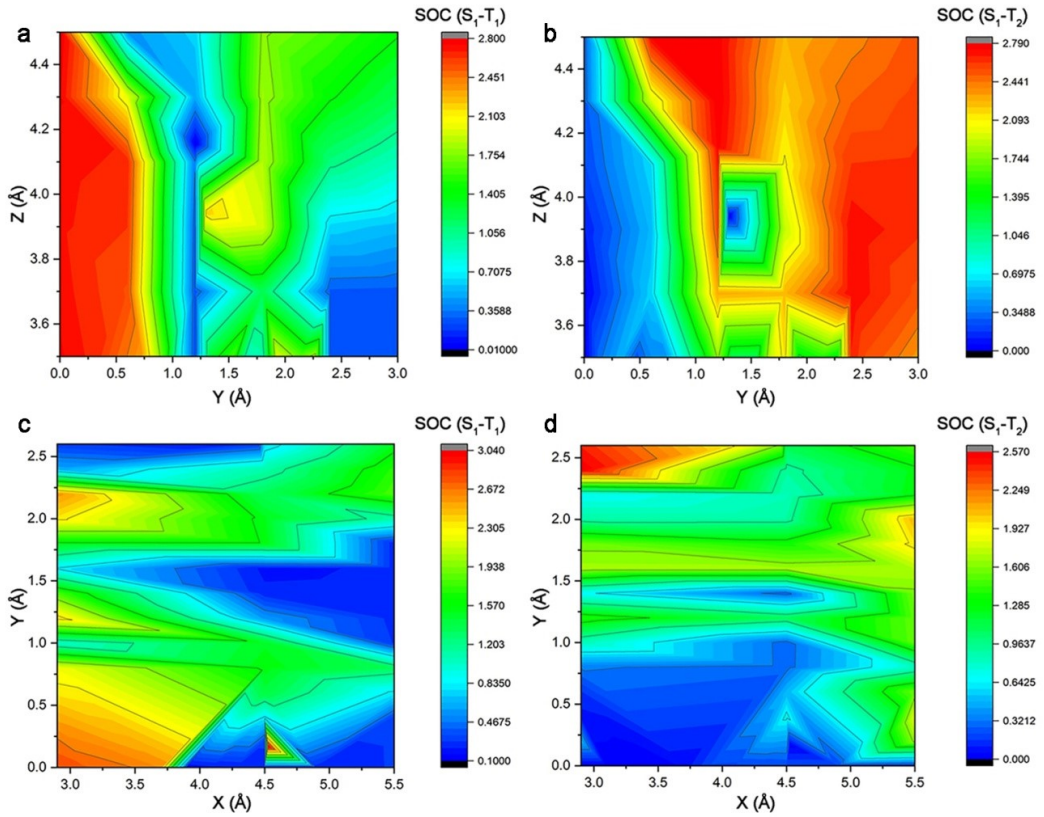

Figure S24. a) Spin-orbit coupling values between S_1 and T_1 and b) S_1 and T_2 with the shifts along Y and Z axes when the shift along X axis is set as 2.9 Å. c) Spin-orbit coupling values between S_1 and T_1 and d) S_1 and T_2 with the shifts along X and Y axes when the shift along Z axis is set as 3.4 Å.

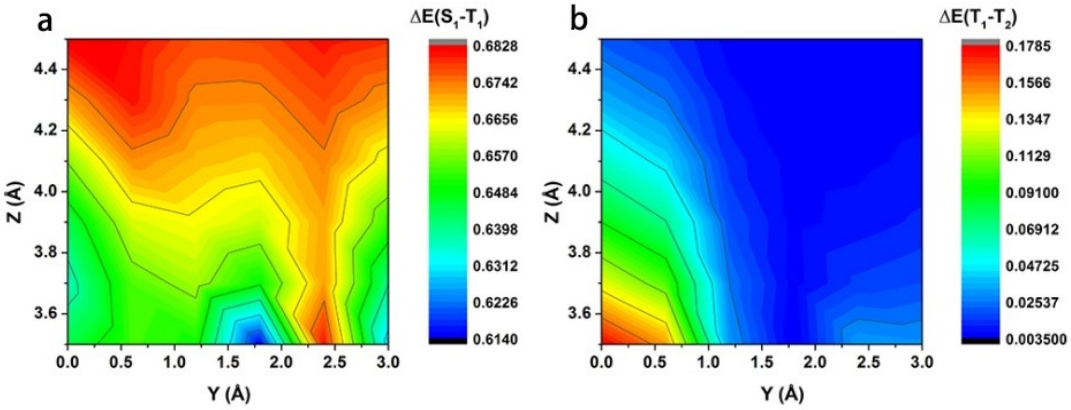

Figure S25. The excitation energies change of S_1, T_1, and T_2 together with their energy gaps with the shift along the Y and Z axes when the shift along the X-axis is set as 2.9 Å.

References

1 M. J. Frisch, G. W. Trucks, H. B. Schlegel, G. E. Scuseria, M. A. Robb, J. R. Cheeseman, G. Scalmani, V. Barone, G. A. Petersson, H. Nakatsuji, X. Li, M. Caricato, A. V. Marenich, J. Bloino, B. G. Janesko, R. Gomperts, B. Mennucci, H. P. Hratchian, J. V. Ortiz, A. F. Izmaylov, J. L. Sonnenberg, D. W. Young, F. Ding, F. Lipparini, F. Egidi, J. Goings, B. Peng, A. Petrone, T. Henderson, D. Ranasinghe, V. G. Zakrzewski, J. Gao, N. Rega, G. Zheng, W. Liang, M. Hada, M. Ehara, K. Toyota, R. Fukuda, J. Hasegawa, M. Ishida, T. Nakajima, Y. Honda, O. Kitao, H. Nakai, T. Vreven, K. Throssell, J. J. Montgomery, J. E. Peralta, F. Ogliaro, M. J. Bearpark, J. J. Heyd, E. N. Brothers, K. N. Kudin, V. N. Staroverov, T. A. Keith, R. Kobayashi, J. Normand, K. Raghavachari, A. P. Rendell, J. C. Burant, S. S. Iyengar, J. Tomasi, M. Cossi, J. M. Millam, M. Klene, C. Adamo, R. Cammi, J. W. Ochterski, R. L. Martin, K. Morokuma, O. Farkas, J. B. Foresman and D. J. Fox, Gaussian 16, Revision C.01, Wallingford CT: Gaussian Inc, 2019.

2 ADF, SCM, Theoretical Chemistry, Virje Universiteit, Amsterdam, The Netherlands, 2016.

3 M. C. Li, M. Hayashi and S. H. Lin, *J. Phys. Chem. A*, 2011, **115**, 14531-14538.

4 E. C. Mark, J. Christine, C. C. Kim and R. S. Dennis, *J. Chem. Phys.*, 1998, **108**, 4439.

5 Y. C. Duan, Y. Wu, J. L. Jin, D. M. Gu, Y. Geng, M. Zhang and Z. M, Su, *Chemphyschem*, 2017, **18**, 755-62.

6 E. van Lenthe, J. G. Snijders and E. J. Baerends, *J. Chem. Phys.*, 1996, **105**, 6505-6516.